Iran J Sci Technol Trans Mech Eng (2019) 43 (Suppl 1):S537–S549
https://doi.org/10.1007/s40997-018-0176-7

RESEARCH PAPER

Effects of Tooth Modifications on the Mesh and Dynamic Characteristics of Differential Gearbox Used in Electric Vehicle

Chao Xiang[1] · Chaosheng Song[1,2] · Caichao Zhu[1] · Yanxiang Weng[2] · Wanlong Guo[2]

Received: 29 May 2017 / Accepted: 9 May 2018 / Published online: 23 May 2018

Abstract
In order to reduce the vibration and noise for the differential gearbox used in electric vehicle, a coupled gear–shaft–bearing–housing dynamic model was developed considering the elastic support by shaft, bearing and housing. Three tooth modification schemes were proposed to investigate the effects of modification type on the mesh behaviors. Results show that the tooth modification scheme with a combined drum–tooth end modification for lead direction and linear addendum modification for profile direction can make the contact load distribution better. The contact pattern was located in the middle of the tooth, and the maximum contact pressure was decreased by 19% to 937 MPa. And the peak–peak value of transmission error was decreased by 33% for high-speed stage and 26% for intermediate stage. The tooth modifications tend to decrease the acceleration responses obviously, especially for the high-frequency range. The structure noise was reduced about 3.5–4.5 dB in x, y and z directions for the selected bearing locations. The analysis results can be applied to guide the design of electric vehicle differential gearbox with low noise level.

Keywords Electric vehicle · Differential gearbox · Mesh characteristic · Dynamics · Tooth modifications

1 Introduction

In the past years, as an alternative for vehicles with gasoline or diesel engines, electric motor vehicles have received increasing interest due to the favorable effects on both noise and air quality in urban environments. The transmission principle diagram of electric vehicle is shown in Fig. 1. Compared to the conventional vehicles, the clutches attached with torsional shock absorbers are simplified and the differential gearbox is directly connected to the electric motor. However, due to the direct connecting and the high input speed 8000–12000 rpm by the electric motor, the requirements for the higher reliability, lower vibration and noise are increased a lot. Therefore, gaining a more thorough understanding of the tooth modifications and mesh behavior as well as dynamics is much essential to reduce the vibration and noise for the differential gearbox used in electric vehicles.

Recently, there have been extensive studies performed on the dynamic analysis for the gear transmissions (Zimroz et al. 2011; Song et al. 2012, 2013; Hua et al. 2011, 2012). A linear, time-invariant dynamic model of double-helical gear pair systems including shafts and bearing supports was developed, and the dynamic behavior was investigated both experimentally and theoretically (Kang and Kahraman 2015). The dynamic model of the back-to-back two-stage planetary gear system was established, and the transient dynamic characteristics were studied considering the variability of speed in the run-up and run-down regimes (Hammami et al. 2015). The whine noise problems of supercharger timing gears under lightly loaded situation

✉ Chaosheng Song
chaoshengsong@cqu.edu.cn

Chao Xiang
424236969@qq.com

Caichao Zhu
cczhu@cqu.edu.cn

Yanxiang Weng
wengyanx@126.com

Wanlong Guo
gwl888888@163.com

[1] The State Key Laboratory of Mechanical Transmissions, Chongqing University, Chongqing 400044, China

[2] Hangzhou Advance Gearbox Group Co., Ltd, Hangzhou 311203, China

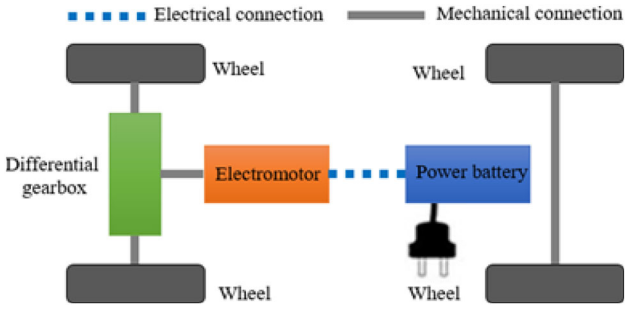

Fig. 1 Transmission principle diagram of electric vehicle

were studied, and new high-contact-ratio spur gear designs were conducted which reduced the gear whine levels by more than 6 dB (Glover 2013). The hot deflection test using an actual gear mounting and the temperature of a cast-aluminum axle housing were performed, and results showed that the contact pattern extended to the tooth boundaries without showing a concentration under peak load conditions (Choi et al. 2012). A combined experimental and numerical investigation of axle whine in a rear-wheel-drive light truck were presented, and results show that a number of modes are excited for vehicle coasting conditions, which can interact with the vibrations of the hypoid gear pair (Koronias et al. 2011). The nonlinear dynamic characteristics of hypoid gear transmission system were studied using improved harmonic balance method (Yang et al. 2014). The interactions between backlash nonlinearity and time-varying meshing stiffness were investigated using multiscale method and numerical method (Kahraman and Singh 1991).

Also a lot of researches have been performed on the dynamic analysis and noise reduction for electric vehicle (Mammetti and Arroyos 2014; Xiong and Huang 2009). A method to evaluate the sound quality of the warning sound masked by background noise considering the masking effect was developed for electric vehicle (Lee et al. 2017). Then, quarter vehicle-electric wheel system dynamics model based on the rigid ring tire assumption was established and the main parameters of the model were identified according to tire free modal test (Mao et al. 2017). A system-simulation-based universal modeling approach for NVH-simulation of electric drive was proposed implementing generic reduced electrodynamic and acoustic models in a system-simulation environment (Kotter et al. 2016). A comparison between transfer path analysis and operational path analysis methods using an electric vehicle was presented considering structure-borne noise paths to the cabin from different engine and suspension points (Diez-Ibarbia et al. 2017). The internal dynamic excitations of a certain electric power train in rated revolution were analyzed, and a dynamic finite element model considering the electro-magnetic forces was developed (Yu and Zhang 2014; Yu et al. 2015; Fang et al. 2014). Some researchers considered the specific tooth modification, but little discussed the effects of different tooth modification strategies on the dynamics of the differential gearbox used in electric vehicles.

In this paper, based on the transmission principle analysis, a coupled gear–shaft–bearing–housing dynamic model was developed considering the flexibility of housing for the differential gearbox used in electric vehicles. Then, three tooth modification schemes were proposed to investigate the effects of modification type on the contact pattern, transmission error and dynamic response. It can provide the theoretical basis for vibration reduction and noise reduction in high-speed gearbox.

2 Transmission Principle and Dynamic Modeling of the Differential Gearbox

The differential gearbox used in electric vehicle with the input speed 8000–12000 rpm is composed of the high-speed stage, intermediate stage and low-speed stage as shown in Fig. 2. The input power is generated by the electric motor, and it was transited to the input shaft, pinion of the high-speed stage, wheel of the high-speed stage and pinion of the intermediate stage. Then the power is transited to the low-speed stage. The basic gearing parameters of the differential gearbox are shown in Table 1.

Considering the elastic supporting of the housing and the shafts, the systematic dynamic model of the differential

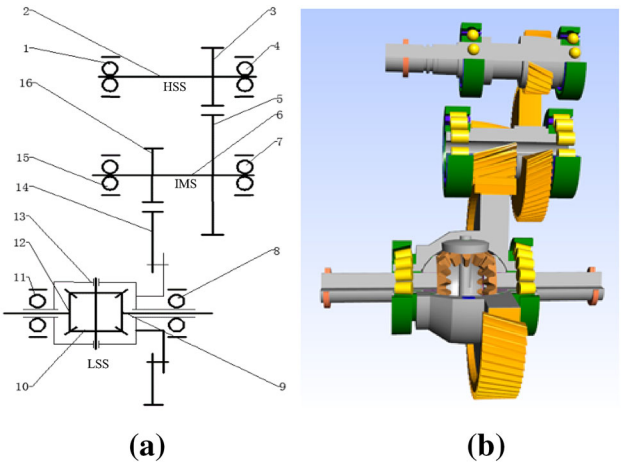

Fig. 2 Structure and transmission principle of the differential gearbox. *Note* HSS, high-speed stage; IMS, intermediate stage; LSS, low-speed stage; 1,4—bearings of high-speed shaft; 2—high-speed shaft; 3—pinion of high-speed stage; 5—wheel of high-speed stage; 6—intermediate shaft; 7,15—bearings of intermediate shaft; 8,11—bearings of output shaft; 9,12—half axle gear; 10—plant; 13—housing of differential; 16—pinion of intermediate stage; 14—wheel of intermediate stage. **a** Transmission diagram. **b** Structural diagram

Table 1 Transmission parameters of the differential gearbox

Parameter	First stage		Second stage		Differential stage	
	Pinion	Wheel	Pinion	Wheel	Plant	Sun
Number of tooth	23	60	21	70	10	16
Module/(mm)	2	2	2.75	2.75	3.9	3.9
Helix angle/(°)	22.5	22.5	18	18	–	–
Pressure angle/(°)	20	20	20	20	22	22
Transmission ratio	2.609		3.333		–	

gearbox was developed using the commercial software Masta as shown in Fig. 3, and the kinetic equation of the dynamic model can be represented by

$$[M]\left\{\ddot{\theta}\right\} + [C]\left\{\dot{\theta}\right\} + [K]\{\theta\} = \{p\} \tag{1}$$

where $[M]$ is the systematic mass matrix, $[C]$ is the systematic damping matrix, and $[K]$ is the systematic stiffness matrix.$\{\theta\}$, $\left\{\dot{\theta}\right\}$ and $\left\{\ddot{\theta}\right\}$ represent the displacement, velocity and acceleration vectors. $\{p\}$ is the external load vector.

Specified bearings were used to connect the housing and the geared rotor system to transit the reaction force and displacement response. To consider the elastic support of the housing, coupling nodes were created at the connection position and the supporting stiffness of housing can be replaced by the combined stiffness matrix of the coupling nodes. To generate the supporting stiffness of housing, a finite element model of the housing considering the actual constraints was developed. In the model, the condensation nodes connected to the bearing surfaces were defined as shown in Fig. 4. Since the nodal force and nodal displacement always have a linear relation, the relationship between the force and displacement of each coupling node between housing and the geared rotor system can be expressed by

$$\begin{bmatrix} F_x \\ F_y \\ F_z \\ M_x \\ M_y \\ M_z \end{bmatrix} = \begin{bmatrix} k_{11} & k_{12} & k_{13} & k_{14} & k_{15} & k_{16} \\ k_{21} & k_{22} & k_{23} & k_{24} & k_{25} & k_{26} \\ k_{31} & k_{32} & k_{33} & k_{34} & k_{35} & k_{36} \\ k_{41} & k_{42} & k_{43} & k_{44} & k_{45} & k_{46} \\ k_{51} & k_{52} & k_{53} & k_{54} & k_{55} & k_{56} \\ k_{61} & k_{62} & k_{63} & k_{64} & k_{65} & k_{66} \end{bmatrix} \begin{bmatrix} \mu_x \\ \mu_y \\ \mu_z \\ \theta_x \\ \theta_y \\ \theta_z \end{bmatrix} \tag{2}$$

where F_x, F_y and F_z represent the force along x, y and z direction, respectively. M_x, M_y and M_z represent the moment along x-, y- and z-axes, respectively. μ_x, μ_y and μ_z represent the translational displacement along x-, y- and z-axes, respectively. θ_x, θ_y and θ_z represent the angular displacement along x-, y- and z-axes, respectively.

Since a total of 6 bearings are used in the differential gearbox, the equivalent supporting stiffness matrix should be 36×36. The relationship between the force and displacement for the housing can be represented by

$$[F]^{(36\times1)} = [K]^{(36\times36)}[\mu]^{(36\times1)} \tag{3}$$

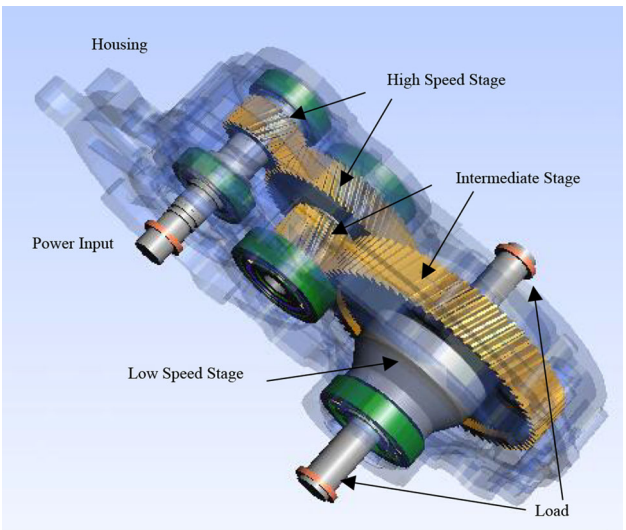

Fig. 3 Systematic dynamic model of the differential gearbox

3 Tooth Modifications and Transmission Error Analysis

Tooth modification is an effective way to reduce the impacts during mesh in and out which tends to decrease the vibration and noise for gear transmissions. The amounts of relief along the tooth width and profile direction are determined by the loads. However, if only one load level was considered to determine the tooth modification, that may worsen the vibration and noise when the load condition changes. Therefore, a wide range of load and speed range (Chen et al. 2014) should be considered to determine the tooth modifications. According to the test load spectrum of differential gearbox used in electric vehicle as shown in Table 2, the lead relief and profile relief were calculated and determined by the following formulas. The length and the maximum amount of crowned relief can be determined by

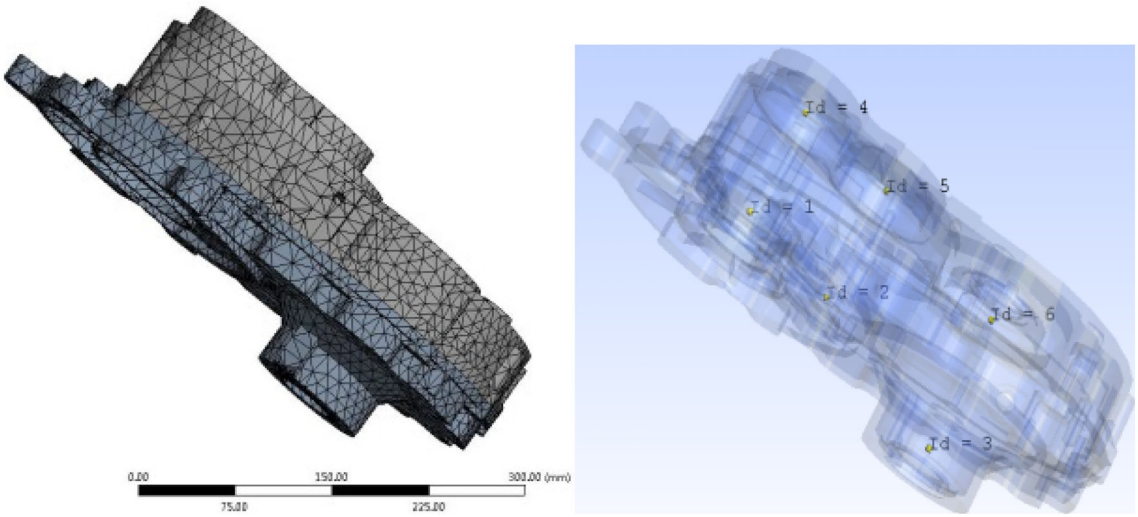

(a) (b)

Fig. 4 Housing model. **a** Finite element model. **b** Condensed nodes

Table 2 Three forward and reverse load situations for the differential gearbox

	Torque(N m)	Number of cycle	Speed (rpm)	Time (h)
Forward load	225	9,269,860	4200	65
	110	12,364,000	8000	50
	70	73,742,880	12,000	175
Reverse load	140	6,951,118	4200	6
Total	–	–	–	296

$$\lambda = P_b(\varepsilon_\alpha - 1) \tag{4}$$

$$e_k = f_{KT} + f_m \tag{5}$$

$$f_m = f_{Pb} + {}^1\!/\!_3 f_f \tag{6}$$

where λ is the length of modification, P_b is the base pitch of gear and ε_α is the transverse contact ratio. e_k is the maximum amount of modification, f_{KT} is the elastic deformation, f_m is the manufacturing error, f_{Pb} is the base pitch error, and f_f is the tooth profile error.

For tooth lead direction, the amounts of crowning relief can be calculated by

$$\delta = 7 \times 10^{-3} \frac{F_t}{b} \tag{7}$$

where δ is the crowning relief, F_t is the tangential mesh force, and b is the tooth width.

The schematic diagrams of gear modifications for profile and lead directions are shown in Fig. 5.

According to the above formulas, the tooth modifications were determined considering three forward and reverse load situations as shown in Table 2. Also, three tooth modification schemes are shown in Table 3 which were proposed to investigate the effects of modification on the contact behaviors. The basic parameters of the lead and profile modifications for gear tooth surface are defined as shown in Figs. 6 and 7. The detailed tooth modification curves in both lead and profile direction are shown in Figs. 8 and 9. The detailed modification parameters are shown in Table 4. Then, the mesh characteristics were analyzed and calculated.

Then, the contact patterns were calculated as shown in Figs. 10, 11, 12 and 13.

From the results, a relative higher contact pressure and obvious edge contact existed for the original scheme without tooth modifications due to the shaft deflection by load. The proposed tooth modification schemes not only increase the effective contact area, but also decrease the maximum value of the contact pressure. For the first scheme, contact pattern along the tooth profile direction shows a good contact stress distribution. However, for the tooth width direction, obvious edge contact can be found for the tooth ends. For the second scheme, obvious edge contact can be found for both the top edge and tooth root along the tooth profile direction. Compared with the first and second tooth modification schemes, the third scheme can make the contact load distribution better with the contact pattern located in the middle of the tooth for both the tooth profile

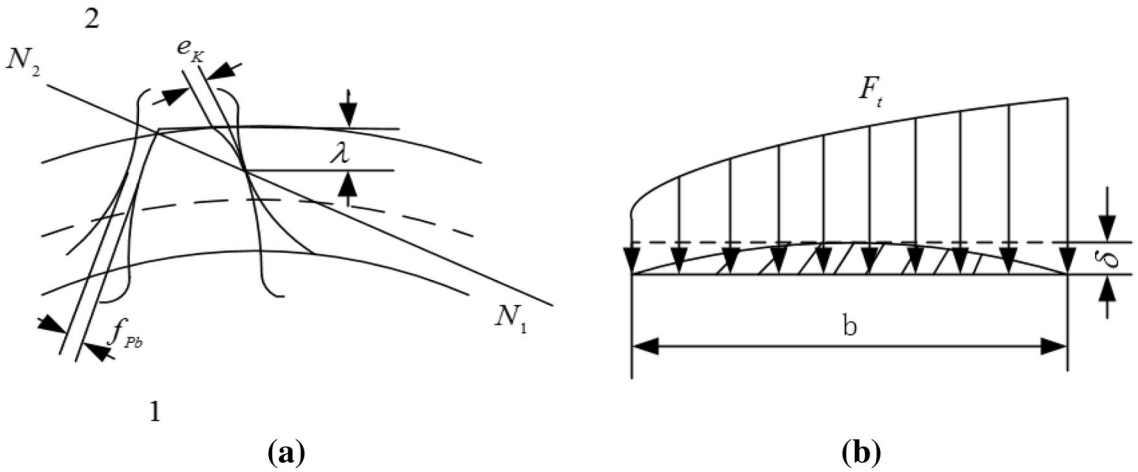

Fig. 5 Schematic diagrams for gear tooth modification. **a** Profile modification. **b** Lead modification

Table 3 Schemes for the tooth modification

Schemes	Lead modification	Profile modification
1	Linear modification	Linear and addendum modification
2	Drum and tooth end modification	Linear modification
3	Drum and tooth end modification	Linear and addendum modification

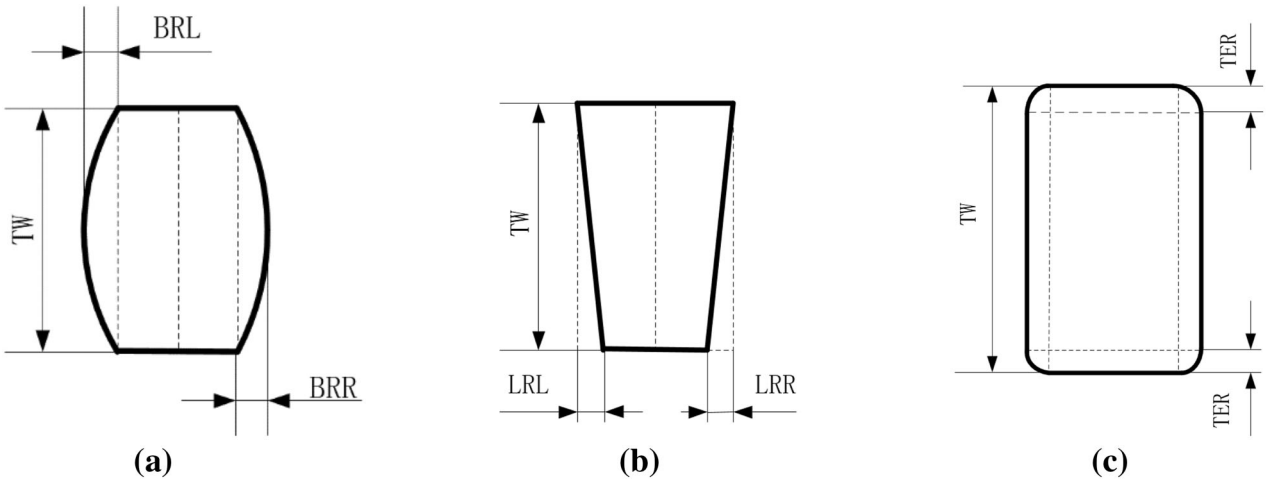

Fig. 6 Basic parameters for lead modification. **a** Drum modification. **b** Linear modification. **c** Tooth end modification

and tooth width direction and the maximum contact pressure decreased by 19% to 937 MPa. The transmission error for the time-varying and peak–peak value are shown in Figs. 14 and 15 for different tooth modification schemes.

From the transmission error results shown above, it can be seen that the time-varying transmission errors are in parabolic shape for both the high-speed and intermediate stages in one mesh cycle and the peak–peak value of transmission error at intermediate stage is obviously higher than that at high-speed stage due to the torque load increase. For the high-speed stage, the peak–peak value of the transmission error from the proposed 3 schemes is smaller than the original scheme. For the intermediate stages, the second and third schemes are better than the original and first schemes. Taking the two stages into account, the third scheme with the least peak–peak value of transmission error is better. The peak–peak values of the transmission error are shown in Table 5. Then, third tooth modification scheme will be used to calculate and analyze the dynamic response subsequently.

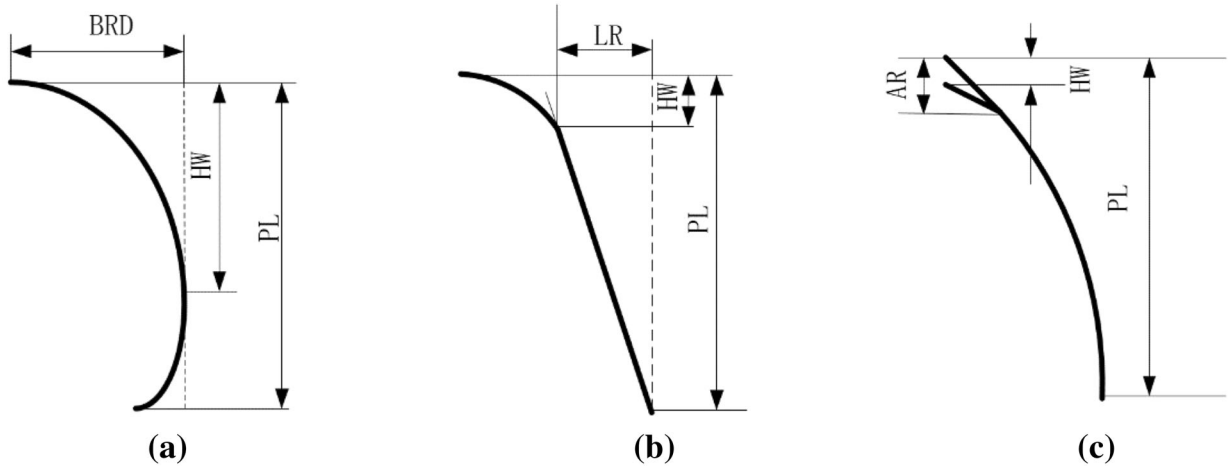

Fig. 7 Basic parameters for profile modification. **a** Barreling modification. **b** Linear modification. **c** Addendum modification

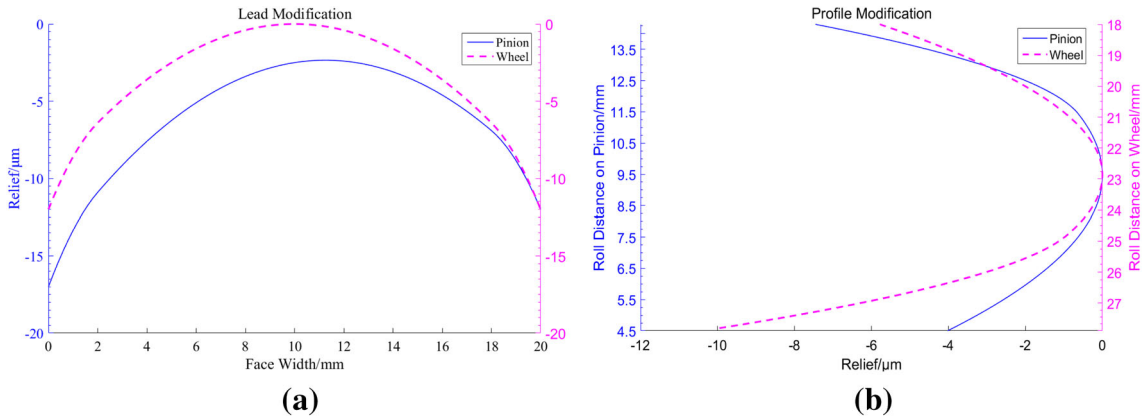

Fig. 8 Gear tooth modification of high-speed stage. **a** Lead direction. **b** Profile direction

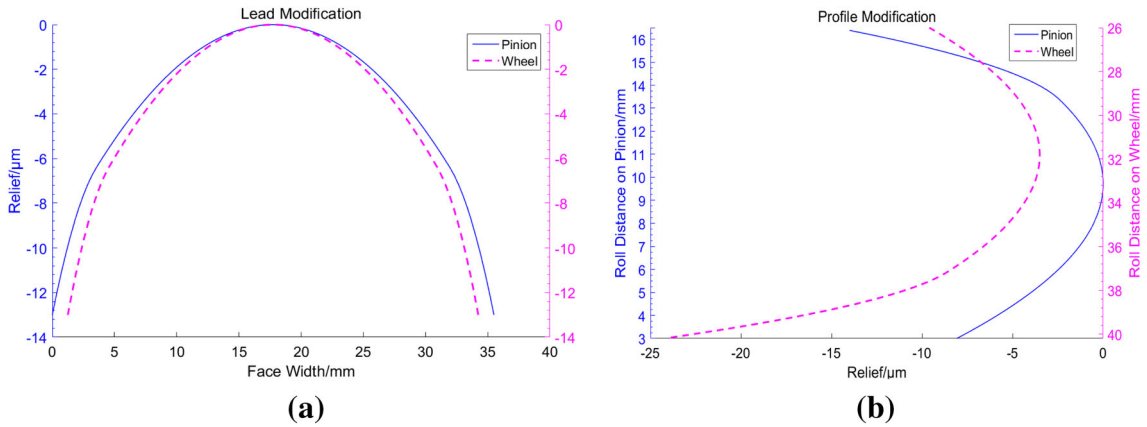

Fig. 9 Gear tooth modification of intermediate stage. **a** Lead direction. **b** Profile direction

4 Dynamic Response Analysis

Radiation noise of gearbox can be divided into airborne noise and structural borne noise, in which the structural noise is 85–90% of the noise energy. Subsequently, the influences of tooth modifications on the structural noise will be investigated. For the differential gearbox here, the input working speed is much higher about 8000–12000 rpm. The first-order mesh frequency of the corresponding input stage is up to 5 kHz and 10 kHz for the

Table 4 Tooth modification parameters

Scheme	Modification parameters (mm)		Modification parameters (μm)			
1						
HSS						
Lead	TW1	TW2	BR1	BR2	LR1	LR2
	22	20	0	0	6	6
Profile	PL	HW	LR1	LR2	AR1	AR2
	9.916	2.95	4	4	2	2
IMS						
Lead	TW1	TW2	BR1	BR2	LR1	LR2
	35.5	33	0	0	8	8
Profile	PL	HW	LR1	LR2	AR1	AR2
	13.351	2.95	8	8	4.2	4.2
2						
HSS						
Lead	TW1	TW2	BR1	BR2	TER1	TER2
	22	20	10	10	4	4
Profile	PL	HW	LR1	LR2	AR1	AR2
	9.916	2.95	4	4	0	0
IMS						
Lead	TW1	TW2	BR1	BR2	TER1	TER2
	35.5	33	15	15	8	8
Profile	PL	HW	LR1	LR2	AR1	AR2
	13.351	2.95	8	8	0	0
3						
HSS						
Lead	TW1	TW2	BR1	BR2	TER1	TER2
	22	20	10	10	4	4
Profile	PL	HW	LR1	LR2	AR1	AR2
	9.916	2.95	4	4	2	2
IMS						
Lead	TW1	TW2	BR1	BR2	TER1	TER2
	35.5	33	15	15	8	8
Profile	PL	HW	LR1	LR2	AR1	AR2
	13.351	2.95	8	8	4.2	4.2

TW tooth width, *PL* effective length of involute, *HW* evaluation parameter, *BR* drum relief, *LR* linear relief, *AR* addendum relief, *TER* tooth end relief

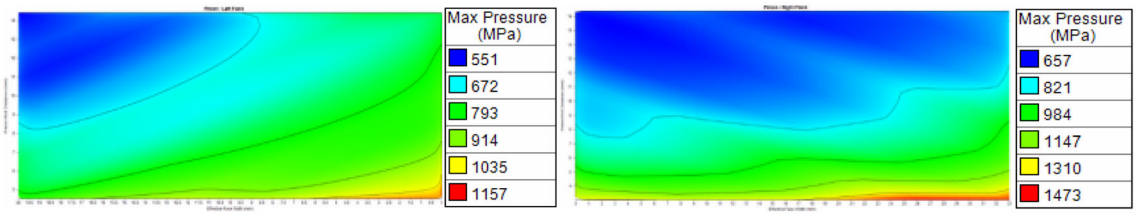

Fig. 10 Contact patterns for original scheme. **a** High-speed stage. **b** Intermediate stage

second order. By performing the dynamic simulation, the dynamic responses on the locations of the 6 bearings were calculated and analyzed under the rated load conditions. It indicated that the right bearing of the high-speed shaft and

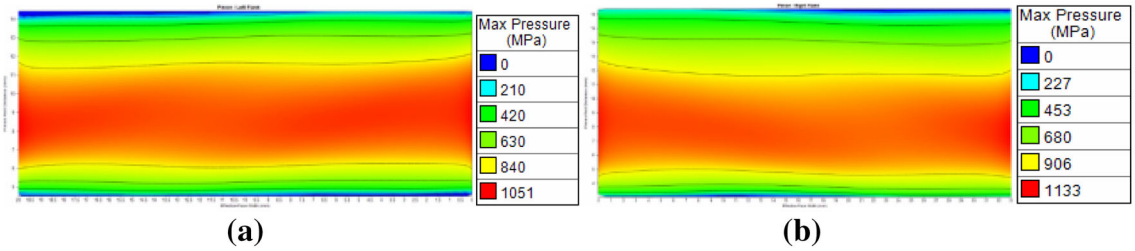

Fig. 11 Contact patterns of 1st scheme. **a** High-speed stage. **b** Intermediate stage

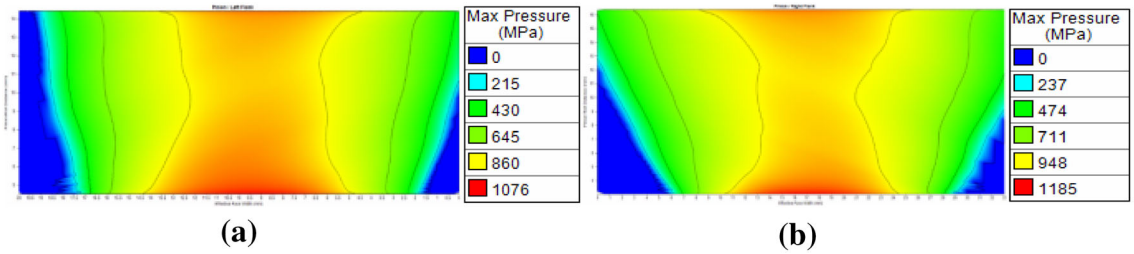

Fig. 12 Contact patterns of 2nd scheme. **a** High-speed stage. **b** Intermediate stage

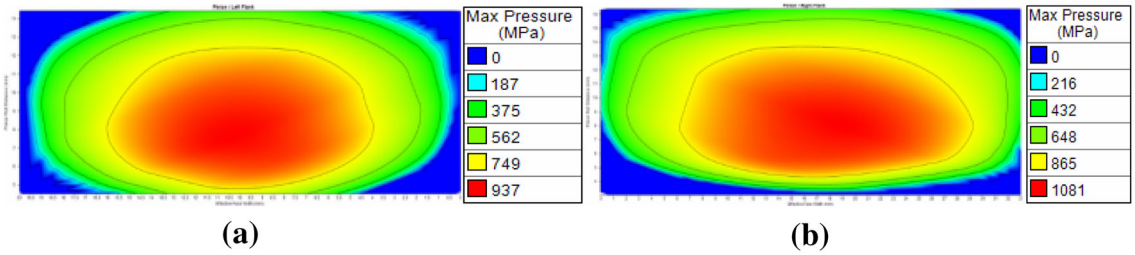

Fig. 13 Contact patterns of 3rd scheme. **a** High-speed stage. **b** Intermediate stage

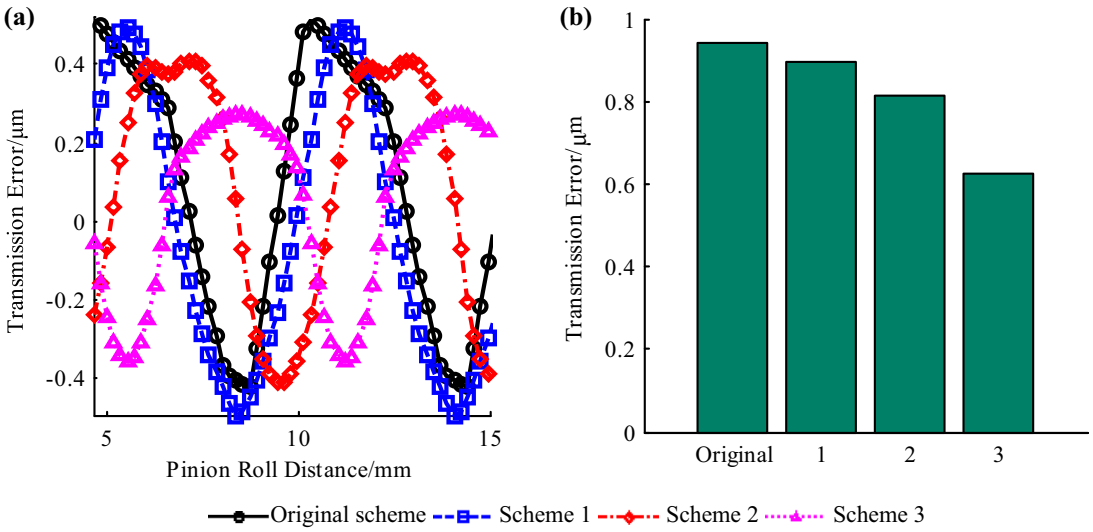

Fig. 14 Transmission error of high-speed stage. **a** Time-varying transmission error. **b** Peak–peak value of transmission error

the right bearing of the intermediate shaft showed a higher vibration response than other locations. The acceleration responses of the two bearing locations in frequency domain are shown in Figs. 16 and 17. Then, based on the acceleration response, the structure noise can be calculated by

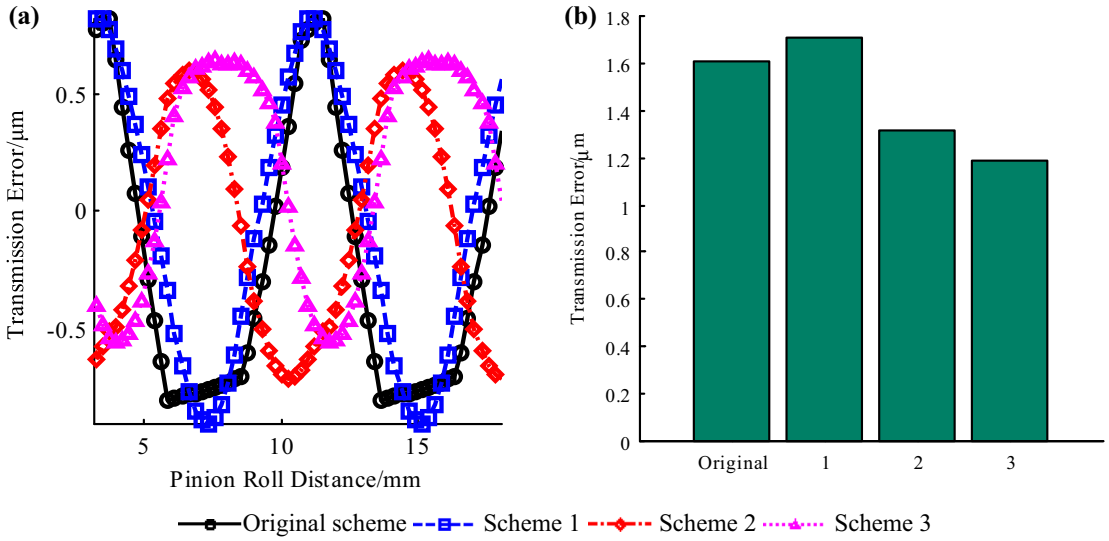

Fig. 15 Transmission error of intermediate stage. **a** Time-varying transmission error. **b** Peak–peak value of transmission error

Table 5 Peak–peak values of transmission error

Scheme	High-speed stage (μm)	Reduction rating	Intermediate stage (μm)	Reduction rating
Original scheme	0.9397	–	1.6133	–
1st scheme	0.8958	4%	1.7168	− 6%
2nd scheme	0.8162	12%	1.3162	18%
3rd scheme	0.6256	33%	1.1932	26%

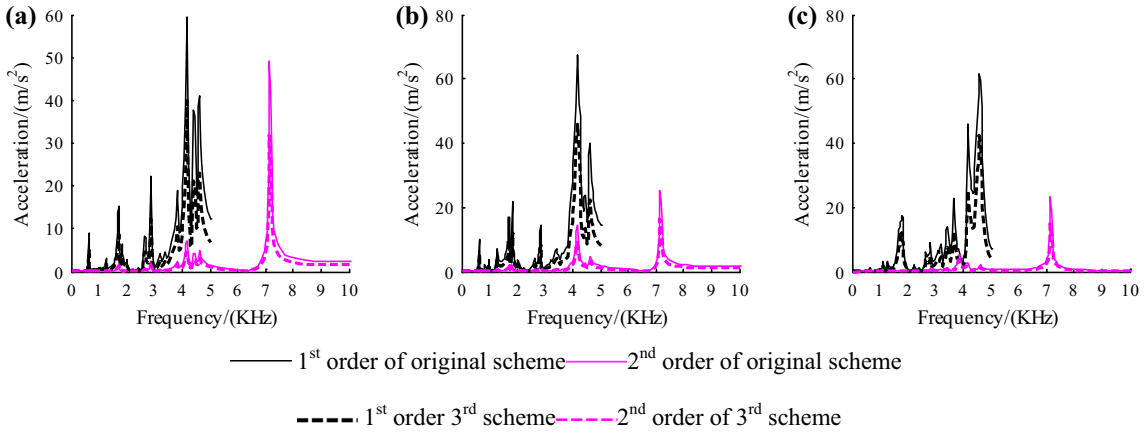

Fig. 16 Acceleration response of right bearing of high-speed shaft. **a** *x* direction. **b** *y* direction. **c** *z* direction

the following formula and the calculated structure noise for the two key locations is shown in Figs. 18 and 19.

$$L_a = 10\log\frac{a^2}{a_0^2} = 20\log\frac{a}{a_0} \tag{8}$$

where L_a is the structure noise, a is the effective value of the acceleration of the frequency band centered at a certain frequency, and a_0 is the reference acceleration, $a_0 = 1 \times 10^{-6}$.

From the results, the acceleration responses in *x*, *y* and *z* directions were decreased obviously by performing the tooth modifications, especially for the high-frequency range. From Figs. 16 and 17, the first-order maximum acceleration responses were decreased from 59.4 to 39.9 m/s^2 in *x* direction, 67.4 to 45.2 m/s^2 in *y* direction

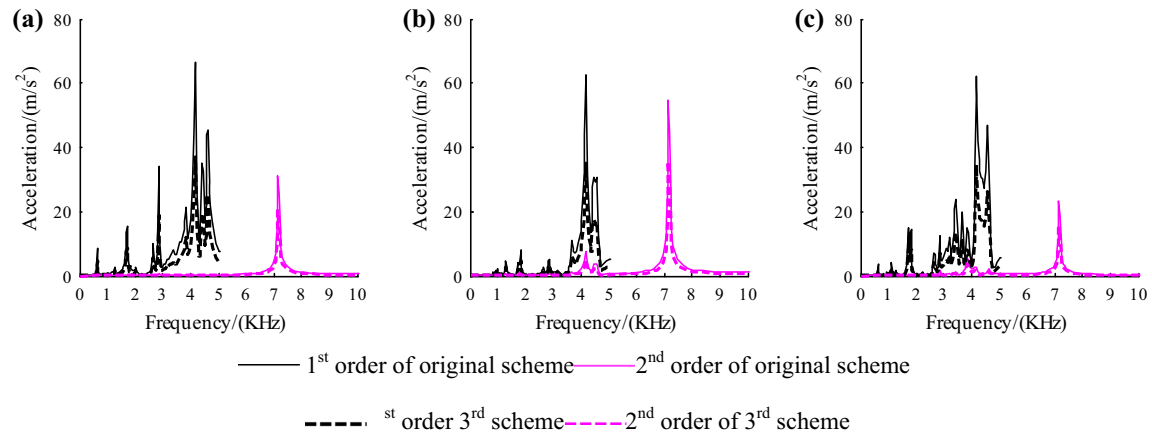

Fig. 17 Acceleration response of right bearing of intermediate shaft. **a** *x* direction. **b** *y* direction. **c** *z* direction

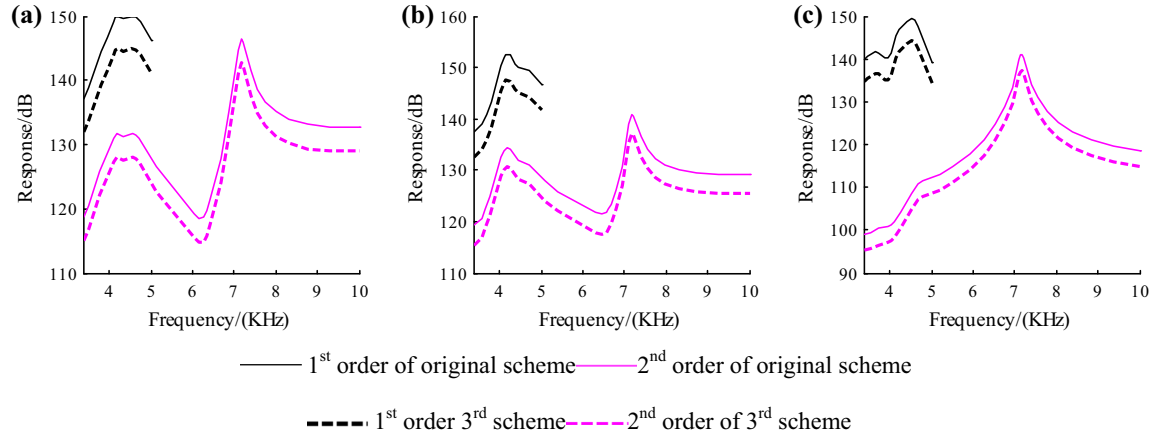

Fig. 18 Structural noise of right bearing of intermediate shaft in enlarged view. **a** *x* direction. **b** *y* direction. **c** *z* direction

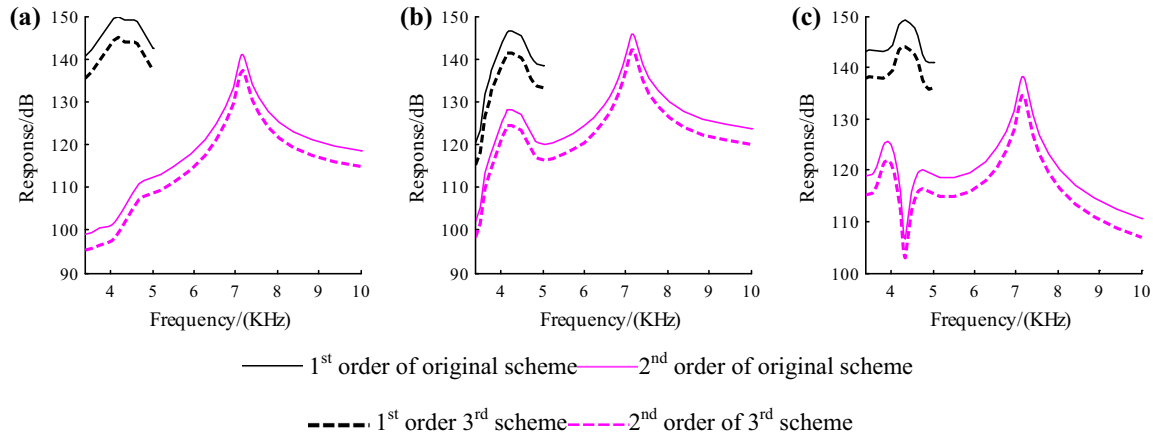

Fig. 19 Structural noise of right bearing of intermediate shaft. **a** *x* direction. **b** *y* direction. **c** *z* direction

and 60.2 to 42.3 m/s^2 in *z* direction for right bearing location of the high-speed shaft; the second-order maximum acceleration responses were decreased from 49.1 to 32.0 m/s^2 in *x* direction, 25.2 to 16.4 m/s^2 in *y* direction and 23.3 to 15.2 m/s^2 in *z* direction for right bearing location of the high-speed shaft. For the right bearing location of the intermediate shaft, the first-order acceleration responses were decreased from 66.4 to 38.0 m/s^2 in *x* direction, 58.7 to 37.8 m/s^2 in *y* direction and 61.8 to 34.5 m/s^2 in *z* direction; the second-order acceleration

Table 6 Maximum acceleration response of the key bearing locations

Acceleration (m/s^2)	High-speed shaft		Intermediate shaft		Output shaft	
	Left bearing	Right bearing	Left bearing	Right bearing	Left bearing	Right bearing
X						
1^{order}						
Original scheme	35.5	59.4	46.1	66.4	38.7	47.2
3rd scheme	22.9	39.9	29.5	37.0	24.2	29.6
2^{order}						
Original scheme	10.3	49.1	12.1	31.3	12.6	19.2
3rd scheme	8.4	32.0	9.5	20.4	8.5	13.5
Y						
1^{order}						
Original scheme	41.7	67.4	46.7	58.7	42.8	39.3
3rd scheme	27.7	45.2	28.2	37.8	29.8	20.8
2^{order}						
Original scheme	10.3	25.2	13.1	54.7	11.9	10.1
3rd scheme	8.1	16.4	8.6	35.7	7.6	7.2
Z						
1^{order}						
Original scheme	35.2	60.2	44.4	61.8	50.8	43.1
3rd scheme	22.6	42.3	25.9	34.5	36.8	26.0
2^{order}						
Original scheme	13.4	23.3	11.9	23.3	13.2	14.6
3rd scheme	10.6	15.2	7.8	15.1	9.5	9.8

responses were decreased from 31.3 to 20.4 m/s^2 in *x* direction, 54.7 to 35.7 m/s^2 in *y* direction and 23.3 to 15.1 m/s^2 in *z* direction. Since the first-order response contains more energy than the second order, a greater peak value can be found for the first-order than the second-order acceleration response. From Figs. 18 and 19, it can be seen that the maximum structure noise in the selected frequency range is reduced about 4 dB in *x*, *y* and *z* directions for the right bearing location of the high-speed shaft, respectively. For the right bearing location of the intermediate shaft, the maximum structure noise in the selected frequency range is reduced about 3–5 dB. Then, the maximum acceleration response and structural noise for other key bearing locations are shown in Tables 6 and 7. It can be seen that the tooth modifications tends to decrease the acceleration response and structural noise obviously.

5 Conclusions

1. Based on the structure and transmission principle analysis, a coupled gear–shaft–bearing–housing dynamic model was developed considering the flexibility of housing for the differential gearbox used in electric vehicles.
2. Three tooth modification schemes were proposed to investigate the effects of modification type on the mesh behaviors. By performing the tooth contact analysis, the tooth modification scheme with a combined drum–tooth end modification for lead direction and linear addendum modification for profile direction can make the contact load distribution better. The contact pattern was located in the middle of the tooth, and the maximum contact pressure was decreased by 19% to 937 MPa. And the peak–peak value of transmission error was decreased by 33% for high-speed stage and 26% for intermediate stage.
3. The effects of tooth modifications on the acceleration response and structure noise were investigated. The tooth modifications tend to decrease the acceleration responses obviously, especially for the high-frequency range. The structure noise was reduced about 3.5–4.5 dB in *x*, *y* and *z* direction for the selected bearing locations. The results can be used as reference

Table 7 Maximum structural noise of the key bearing locations

Structural noise (dB)	High-speed shaft		Intermediate shaft		Output shaft	
	Left bearing	Right bearing	Left bearing	Right bearing	Left bearing	Right bearing
X						
1^{order}						
Original scheme	142.9	150.0	145.0	150.0	143.1	145.1
3rd scheme	140.6	146.4	141.0	145.3	140.5	141
NRR	2.3	3.6	4.0	4.7	2.6	4.1
2^{order}						
Original scheme	135.2	144.9	135.9	140.8	135.9	139.2
3rd scheme	134.3	142.7	134.8	137.2	134.3	136.2
NRR	0.9	2.2	1.1	3.6	1.6	3.0
Y						
1^{order}						
Original scheme	144.3	152.6	145.1	148.6	143.8	143.3
3rd scheme	140.9	148.8	140.8	144.1	141.6	139.0
NRR	3.4	3.8	4.3	4.5	2.2	4.3
2^{order}						
Original scheme	135.2	140.6	136.0	145.2	135.9	135.0
3rd scheme	134.2	137.3	134.4	142.0	134.2	134.1
NRR	1.0	3.3	1.6	3.2	1.7	0.9
Z						
1^{order}						
Original scheme	142.9	149.3	144.8	149.2	145.0	143.9
3rd scheme	140.5	144.8	140.7	145.0	143.0	140.7
NRR	2.4	4.5	4.1	4.2	2.0	3.2
2^{order}						
Original scheme	136.1	140.5	135.9	140.8	136.1	136.8
3rd scheme	135.3	137.1	134.1	136.6	134.8	134.9
NRR	0.8	3.4	1.8	4.2	1.3	1.9

NRR noise reduction rating

for the control of the noise of gearbox of electric vehicle in the future.

Acknowledgement The authors would like to thank the National Natural Science Foundation of China (No. 51775061), Chongqing Research Program of Basic Research and Frontier Technology (No. cstc2016jcyjA0415), Postdoctoral Special Projects Funded of Chongqing (No. Xm2016004) and Fundamental Research Funds for Central Universities (106112017CDJPT280002).

References

Chen SY, Tang JY et al (2014) Effect of modification on dynamic characteristics of gear transmission system. J Mech Eng 50(13):59–65

Choi BJ, Yoon JH, Oh JE (2012) A study on axle gear whine noise reduction with deflection test. Proc Inst Mech Eng Part D J Automob Eng 226(D2):225–233

Diez-Ibarbia A, Battarra M, Palenzuela J, Cervantes G, Walsh S et al (2017) Comparison between transfer path analysis methods on an electric vehicle. Appl Acoust 118:83–101

Fang Y, Zhang T, Yu P, Guo R (2014) Research and analysis of the internal excitations of electric powertrain. J Vib Meas Diagn 34(3):496–502

Glover R (2013) Design of high speed gears, low load gears for minimizing gear whine noise. In: Proceedings of the ASME international design engineering technical conferences and computers and information in engineering conference, August 4–7, Portland, Oregon, USA

Hammami A, Del Rincon AF, Chaari F, Rueda FV, Haddar M (2015) Dynamic behavior of back to back planetary in run up and run down transient regimes. J Mech 31(4):481–491

Hua X, Lim TC, Peng T (2011) Effect of shaft-bearing configurations on spiral bevel gear mesh and dynamics. In: SAE noise and vibration conference, Grand Rapids, MI, USA

Hua X, Lim TC, Peng T, Wali WE (2012) Dynamic analysis of spiral bevel geared rotor systems applying finite elements and enhanced lumped parameters. Int J Autom Technol 13(1):97–107

Kahraman A, Singh R (1991) Interactions between time-varying meshing stiffness and clearance non-linearities in a geared system. J Sound Vib 146(1):135–156

Kang MR, Kahraman A (2015) An experimental and theoretical study of the dynamic behavior of double-helical gear sets. J Sound Vib 350(18):11–29

Koronias G, Theodossiades S, Rahnejat H, Saunders T (2011) Axle whine phenomenon in light trucks: a combined numerical and experimental investigation. Proc Inst Mech Eng Part D J Automob Eng 225(D7):885–894

Kotter P, Zim O, Wegener K (2016) Efficient noise–vibration–harshness modelling of servo- and traction drives. In: 7th IFAC symposium on mechatronic systems, Loughborough Univ, Leicestershire, England, vol 49, no 21, pp 330–338

Lee SK, Lee SM, Shin T, Han M (2017) Objective evaluation of the sound quality of the warning sound of electric vehicles with a consideration of the masking effect: annoyance and detectability. Int J Automot Technol 18(4):699–705

Mammetti M, Arroyos MR (2014) The study of torque control characterstics for the optimization of the NVH of an electric vehicle. In: SAE 2014 world congress & exhibition, April 8–10, Detroit, Michigan, USA

Mao Y, Zuo SG, Wu SD, Duan XL (2017) High frequency vibration characteristics of electric wheel system under in-wheel motor torque ripple. J Sound Vib 400(21):442–456

Song CS, Zhu CC, Lim TC, Peng T (2012) Parametric analysis of gear mesh and dynamic response of loaded helical beveloid transmission with small shaft angle. J Mech Des 134(8):1–8

Song CS, Zhu CC, Liu WJ (2013) Sliding friction effect on dynamics of crossed beveloid gears with small shaft angle. J Mech Sci Technol 27(5):1255–1263

Xiong J, Huang J (2009) Analysis and control of noise and vibration of hybrid electric vehicles. Noise Vib Control 29(5):96–100

Yang JY, Peng T, Lim TC (2014) An enhanced multi-term harmonic balance solution for nonlinear period-dynamic motions in right-angle gear pairs. Nonlinear Dyn 76(2):1237–1252

Yu P, Zhang T (2014) Investigation on modeling method of powertrain mounting system of central driven electric vehicle. Chin J Constr Mach 6(1):471–477

Yu P, Chen FF, Zhang T, Guo R (2015) Vibration characteristics analysis of a central-drive electric vehicle powertrain. J Vib Shock 34(1):44–48

Zimroz R, Urbanek J, Barszcz T et al (2011) Measurement of instantaneous shaft speed by advanced vibration signal processing—application on wind turbine gearbox. Metrol Meas Syst 18(4):701–711